

Enclosure 2 to

W3F1-2010-0003

WCAP-17187-NP, Revision 0,

**Technical Justification for Eliminating Pressurizer Surge Line Rupture as the
Structural Design Basis for Waterford Steam Electric Station, Unit 3,
Using Leak-Before-Break Methodology"
February 2010**

(Non-Proprietary)

Technical Justification for
Eliminating Pressurizer
Surge Line Rupture as the
Structural Design Basis for
Waterford Steam Electric
Station, Unit 3 Using Leak-
Before-Break Methodology

WCAP-17187-NP
Revision 0

**Technical Justification for Eliminating Pressurizer
Surge Line Rupture as the Structural Design Basis for
Waterford Steam Electric Station, Unit 3 Using Leak-
Before-Break Methodology**

February 2010

Anees Udyawar*
Piping Analysis and Fracture Mechanics

Daniel Denis
Reddy Ganta
Major Reactor Component Design & Analysis

Reviewer: Dulal Bhowmick*
Chris Kupper*
Piping Analysis and Fracture Mechanics

Approved: Seth Swamy*, Manager
Piping Analysis and Fracture Mechanics

*Electronically approved records are authenticated in the electronic document management system.

Westinghouse Electric Company LLC
P.O. Box 355
Pittsburgh, PA 15230-0355

© 2010 Westinghouse Electric Company LLC
All Rights Reserved

TABLE OF CONTENTS

1.0	Introduction	1-1
1.1	Background	1-1
1.2	Scope and Objective	1-1
1.3	References	1-2
2.0	Operation and Stability of the Reactor Coolant System	2-1
2.1	Stress Corrosion Cracking	2-1
2.2	Water Hammer	2-2
2.3	Low Cycle and High Cycle Fatigue	2-3
2.4	Summary Evaluation of Surge Line for Potential Degradation During Service	2-3
2.5	References	2-4
3.0	Loads for Fracture Mechanics Analysis	3-1
3.1	Nature of the Loads	3-1
3.2	Loads for Crack Stability Analysis	3-2
3.3	Loads for Leak Rate Evaluation	3-2
3.4	Loading Conditions	3-3
3.5	Summary of Loads	3-4
3.6	Governing Locations	3-4
3.7	References	3-5
4.0	Material Characterization	4-1
4.1	Pipe Material and Welding Process	4-1
4.2	Material Properties	4-1
4.3	References	4-5
5.0	Leak Rate Predictions	5-1
5.1	Introduction	5-1
5.2	General Considerations	5-1
5.3	Calculation Method	5-1
5.4	Leak Rate Calculations	5-2
5.5	References	5-4
6.0	Fracture Mechanics Evaluation	6-1
6.1	Local Failure Mechanism	6-1
6.2	Global Failure Mechanism	6-2
6.3	Stability Evaluation	6-3
6.4	References	6-4
7.0	Fatigue Crack Growth Analysis	7-1
7.1	Methodology	7-1
7.2	Fatigue Crack Growth Results	7-2
7.3	References	7-3

8.0 Assessment of Margins 8-1

9.0 Conclusions 9-1

Appendix A – Limit Moment A-1

LIST OF TABLES

Table 3-1	Critical Location Dimensions (inches)	3-6
Table 3-2	Types of Loadings	3-6
Table 3-3	Normal and Faulted Loading Cases for Leak-Before-Break Evaluations	3-7
Table 3-4	Associated Load Cases for Analyses	3-8
Table 3-5	Summary of Loads and Stresses at the Critical Locations	3-9
Table 3-6	Summary of Loads and Stresses at the SWOL Critical Location	3-10
Table 4-1	Tensile Material Properties for Cast Stainless Steel Base and Stainless Steel Weld Metal at the Critical Locations	4-6
Table 4-2	Tensile Material Properties for Alloy 82/182 and Alloy 52M at the Critical SWOL Location (Node 10)	4-6
Table 4-3	Chemical Composition of Surge Line Component 751-110.....	4-7
Table 4-4	J-resistance Curve Parameters for Cast Austenitic Stainless Steel.....	4-8
Table 4-5	Fracture Toughness Properties used to Evaluate Critical Locations at Cast Austenitic Stainless Steel Surge Line	4-9
Table 5-1	Leakage Flaws for the Leak-Before-Break Analyses at Surge Line Piping Critical Locations	5-8
Table 5-2	Leakage Flaws for the Leak-Before-Break Analyses at SWOL Critical Location (Node 10).....	5-8
Table 6-1	Summary of Critical Flaw Size for Critical Locations	6-5
Table 6-2	Summary of Critical Flaw Size for SWOL Critical Location (Node 10)	6-5
Table 6-3	Stability Results for Waterford 3 Pressurizer Surge Line Based on Elastic-Plastic J-integral Evaluations.....	6-6
Table 7-1	Surge Line Transients.....	7-4
Table 7-2	FCG Results for Pressurizer Surge Line Nozzle Weld Overlay Region	7-6
Table 7-3	FCG Results for Hot Leg Surge Line Nozzle Weld Overlay Region.....	7-6
Table 7-4	FCG Results for Intermediate Surge Line Location (Node 70).....	7-6
Table 8-1	Leakage Flaws, Critical Flaw Sizes and Margins at the Critical Location for Surge Line Piping Based on Limit Load Evaluation.....	8-2
Table 8-2	Leakage Flaw Sizes, Critical Flaw Sizes and Margins for the SWOL Critical Weld Location (Node 10) Based on Limit Load Evaluation	8-2
Table 8-3	Stability Margins for Waterford 3 Pressurizer Surge Line Piping Based on Elastic-Plastic J-integral Evaluations.....	8-3

LIST OF FIGURES

Figure 3-1	Schematic Layout of Waterford 3 Surge Line Showing LBB Analyzed Weld Location by Nodes.....	3-11
Figure 5-1	Analytical Predications of Critical Flow Rates of Steam-Water Mixtures.....	5-5
Figure 5-2	[$\beta^{a,c,e}$] Pressure Ratio as a Function of L/D.....	5-6
Figure 5-3	Idealized Pressure Drop Profile Through a Postulated Crack.....	5-7
Figure 6-1	Fully Plastic Stress Distribution.....	6-7
Figure 6-2	Loads Acting on the Model at the Governing Locations.....	6-8
Figure 6-3	Critical Flaw Size Prediction – Waterford 3 Node 70.....	6-9
Figure 6-4	Critical Flaw Size Prediction – Waterford 3 Node 75.....	6-10
Figure 6-5	Critical Flaw Size Prediction – Waterford 3 Node 20.....	6-11
Figure 6-6	Critical Flaw Size Prediction – Waterford 3 Alloy 82/182 and Alloy 52M Welds.....	6-12
Figure 7-1	Reference Fatigue Crack Growth Curves for Stainless Steel.....	7-7
Figure A-1	Pipe with a Through-Wall Crack In Bending.....	A-2

1.0 INTRODUCTION

1.1 BACKGROUND

The current structural design basis for the pressurizer surge line requires postulating non-mechanistic circumferential and longitudinal pipe breaks. This results in additional plant hardware (e.g. pipe whip restraints and jet shields) that would mitigate the dynamic consequences of the pipe breaks. Presented in this report are the descriptions of a mechanistic pipe break evaluation method and the analytical results that can be used for establishing that a circumferential type break will not occur within the Pressurizer surge line. The evaluations consider that circumferentially oriented flaws cover longitudinal cases. The Pressurizer surge line is known to be subjected to thermal stratification, and the effects of thermal stratification for the Waterford Steam Electric Station, Unit 3 (Waterford 3) have been evaluated and used for the Leak-Before-Break (LBB) analysis.

The purpose of this report is to document the analyses and evaluations performed for the application of the Leak-Before-Break methodology to eliminate consideration of the dynamic effects resulting from pipe breaks in the Pressurizer surge line for Waterford 3. This analysis considers the impact of the Structural Weld Overlay (SWOL) performed on the Pressurizer surge nozzle and the hot leg to surge line nozzle.

1.2 SCOPE AND OBJECTIVE

The objective of this investigation is to demonstrate Leak-Before-Break for the Waterford 3 Pressurizer surge line. The scope of this work covers the entire Pressurizer surge line from the primary loop hot leg nozzle junction to the pressurizer nozzle junction. A schematic drawing of the surge line piping system is shown in Figure 3-1. The recommendations and criteria proposed in SRP 3.6.3 (Reference 1-1) are used in this evaluation. The criteria and the resulting steps of the evaluation procedure can be briefly summarized as follows:

1. Calculate the applied loads. Identify the location(s) at which the highest faulted stress occurs.
2. Identify the materials. For the materials types used in the plant, provide representative material properties. Evaluate the long term effects of thermal aging for the cast stainless steel material.
3. Postulate a through-wall flaw at the governing location(s). The size of the flaw should be large enough so that the leakage is assured of detection with margin using the installed leak detection equipment, when the pipe is subjected to normal operating loads. Demonstrate that there is a margin of 10 between the calculated leak rate and the leak detection capability.
4. Using maximum faulted loads in the stability analysis, demonstrate that there is a margin of 2 between the leakage size flaw and the critical size flaw.

5. Review the operating history to ascertain that operating experience has indicated no particular susceptibility to failure from the effects of corrosion, water hammer or low and high cycle fatigue.
6. Demonstrate margin on applied load by combining the faulted loads by the absolute summation method.
7. Perform fatigue crack growth analysis. Show that a through-wall crack will not result.

This report documents the fracture mechanics demonstration of pressurizer surge line integrity for Waterford 3 based on the LBB methodology (Reference 1-1) and consistent with the NRC position for exemption from consideration of dynamic effects (Reference 1-2).

The leak rate is calculated for the normal operating condition. The leak rate prediction model used in this evaluation is an [

]^{a,c,e} The crack opening area required for calculating the leak rates is obtained by subjecting the postulated through-wall flaw to normal operating loads (Reference 1-3).

It should be noted that the terms "flaw" and "crack" have the same meaning and are used interchangeably. "Governing location" and "critical location" are also used interchangeably throughout the report.

1.3 REFERENCES

- 1-1 NUREG-0800 Revision 1, March 2007, Standard Review Plan: 3.6.3 Leak-Before-Break Evaluation Procedures.
- 1-2 Nuclear Regulatory Commission, 10CFR 50, "Modification of General Design Criteria Requirements for Protection Against Dynamic Effects of Postulated Pipe Ruptures, Final Rule," Federal Register/Vol. 52, No. 207 Tuesday, October 27, 1987/Rules and Regulations, pp. 41288-41295.
- 1-3 Tada, H., "The Effects of Shell Corrections on Stress Intensity Factors and the Crack Opening Area of Circumferential and a Longitudinal Through-Crack in a Pipe," Section II-1, NUREG/CR-3464, September 1983.

2.0 OPERATION AND STABILITY OF THE REACTOR COOLANT SYSTEM

2.1 STRESS CORROSION CRACKING

The Westinghouse and Combustion Engineering (CE) designed reactor coolant system (RCS) primary loops have an operating history that demonstrates the inherent operating stability characteristics of the design. This includes a low susceptibility to cracking failure from the effects of corrosion (e.g., intergranular stress corrosion cracking (IGSCC)). This operating history totals over 1400 reactor-years, including 16 plants each having over 30 years of operation, 10 other plants each with over 25 years of operation, 11 plants each over 20 years of operation and 12 plants each over 15 years of operation.

In 1978, the United States Nuclear Regulatory Commission (USNRC) formed the second Pipe Crack Study Group. (The first Pipe Crack Study Group (PCSG) established in 1975 addressed cracking in boiling water reactors only.) One of the objectives of the second PCSG was to include a review of the potential for stress corrosion cracking in Pressurized Water Reactors (PWR's). The results of the study performed by the PCSG were presented in NUREG-0531 (Reference 2-1) entitled "Investigation and Evaluation of Stress Corrosion Cracking in Piping of Light Water Reactor Plants." In that report the PCSG stated:

"The PCSG has determined that the potential for stress-corrosion cracking in PWR primary system piping is extremely low because the ingredients that produce IGSCC are not all present. The use of hydrazine additives and a hydrogen overpressure limit the oxygen in the coolant to very low levels. Other impurities that might cause stress-corrosion cracking, such as halides or caustic, are also rigidly controlled. Only for brief periods during reactor shutdown when the coolant is exposed to the air and during the subsequent startup are conditions even marginally capable of producing stress-corrosion cracking in the primary systems of PWRs. Operating experience in PWRs supports this determination. To date, no stress corrosion cracking has been reported in the primary piping or safe ends of any PWR."

For stress corrosion cracking (SCC) to occur in piping, the following three conditions must exist simultaneously: high tensile stresses, susceptible material, and a corrosive environment. Since some residual stresses and some degree of material susceptibility exist in any stainless steel piping, the potential for stress corrosion is minimized by properly selecting a material resistant to SCC as well as preventing the occurrence of a corrosive environment. The material specifications consider compatibility with the system's operating environment (both internal and external) as well as other material in the system, applicable ASME Code rules, fracture toughness, welding, fabrication, and processing.

The elements of a water environment known to increase the susceptibility of austenitic stainless steel to stress corrosion are: oxygen, fluorides, chlorides, hydroxides, hydrogen peroxide, and reduced forms of sulfur (e.g., sulfides, sulfites, and thionates). Strict pipe cleaning standards prior to operation and careful control of water chemistry during plant operation are used to

prevent the occurrence of a corrosive environment. Prior to being put into service, the piping is cleaned internally and externally. During flushes and preoperational testing, water chemistry is controlled in accordance with written specifications. Requirements on chlorides, fluorides, conductivity, and pH are included in the acceptance criteria for the piping.

During plant operation, the reactor coolant water chemistry is monitored and maintained within very specific limits. Contaminant concentrations are kept below the thresholds known to be conducive to stress corrosion cracking with the major water chemistry control standards being included in the plant operating procedures as a condition for plant operation. For example, during normal power operation, oxygen concentration in the RCS is expected to be in the ppb (parts per billion) range by controlling charging flow chemistry and maintaining hydrogen in the reactor coolant at specified concentrations. Halogen concentrations are also stringently controlled by maintaining concentrations of chlorides and fluorides within the specified limits. Thus during plant operation, the likelihood of stress corrosion cracking is minimized.

Wall thinning by erosion and erosion-corrosion effects will not occur in the surge line due to the low velocity and the material, austenitic stainless steel, is highly resistant to these degradation mechanisms. Therefore, wall thinning is not a credible concern in the portion of the system being addressed in this evaluation.

During 1979, several instances of cracking in PWR feed water piping led to the establishment of the third PCSCG. The investigations of the PCSCG reported in NUREG-0691 (Reference 2-2) further confirmed that no occurrences of IGSCC have been reported for PWR primary coolant systems.

Primary Water Stress Corrosion Cracking (PWSCC) occurred in V. C. Summer reactor vessel hot leg nozzle, Alloy 82/182 weld. It should be noted that this susceptible material is found at the Waterford 3 Pressurizer surge nozzle and the hot leg to surge line nozzle locations; however, structural weld overlay (SWOL) was implemented to mitigate the PWSCC concern. SWOL is a technique that is used to reinforce the Alloy 82/182 welds in PWR plants susceptible to PWSCC. The reinforcement material (Alloy 52M) forms a structural barrier to PWSCC and produces a compressive residual stress condition at the inner portion of the pipe/weld/fitting that mitigates future crack initiation and/or propagation due to PWSCC.

2.2 WATER HAMMER

Overall, there is a low potential for water hammer in the RCS since it is designed and operated to preclude the voiding condition in normally filled lines. The reactor coolant system, including piping and primary components, is designed for normal, upset, emergency, and faulted condition transients. The design requirements are conservative relative to both the number of transients and their severity. Relief valve actuation and the associated hydraulic transients following valve opening are considered in the system design. Other valve and pump actuations are relatively slow transients with no significant effect on the system dynamic loads. To ensure dynamic system stability, reactor coolant parameters are stringently controlled. Temperature during normal operation is maintained within a narrow range by control rod position; pressure is controlled by Pressurizer heaters and Pressurizer spray also within a narrow range for

steady-state conditions. The flow characteristics of the system remain constant during a fuel cycle because the only governing parameters, namely system resistance and the reactor coolant pump characteristics, are controlled in the design process. Additionally, Westinghouse and CE designs have instrumented typical reactor coolant systems to verify the flow and vibration characteristics of the system. Preoperational testing and operating experience have verified this particular approach. The operating transients of the RCS primary piping are such that no significant water hammer can occur.

2.3 LOW CYCLE AND HIGH CYCLE FATIGUE

Fatigue considerations are accounted for in the surge line piping through the fatigue usage factor evaluation for the stratification analyses to show compliance with the rules of Section III of the ASME Code. An evaluation of the low cycle fatigue loadings was carried out as part of this study in the form of a fatigue crack growth analysis, as discussed in Section 7.0.

Pump vibrations during operation would result in high cycle fatigue loads in the piping system. During operation, an alarm signals the exceeding of the Reactor Coolant Pump (RCP) vibration limits. Field vibration measurements have been made on the reactor coolant loop piping in a number of plants during hot functional testing. Stresses in the elbow below the RCP have been found analytically to be very small, between 2 and 3 ksi at the highest. Field measurements on a typical PWR plant indicate vibration amplitudes less than 1 ksi. When translated to the connecting surge line, these stresses would be even lower, well below the fatigue endurance limit for the surge line material and would result in an applied stress intensity factor below the threshold for fatigue crack growth. Waterford 3 RCS configurations are similar and the results are concluded to be similar.

2.4 SUMMARY EVALUATION OF SURGE LINE FOR POTENTIAL DEGRADATION DURING SERVICE

There has never been any service cracking or wall thinning identified in the pressurizer surge line of Westinghouse and CE PWR design. The design, construction, inspection, and operation of the pressurizer surge line piping mitigate sources of such degradation.

There is no known mechanism for water hammer in the pressurizer/surge system. The pressurizer safety and relief piping system that is connected to the top of the pressurizer could have loading from water hammer events. However, these loads are effectively mitigated by the pressurizer and have a negligible effect on the surge line.

Wall thinning by erosion and erosion-corrosion effects should not occur in the surge line due to the low velocity, typically less than 1.0 ft/sec and the material, austenitic stainless steel, which is highly resistant to these degradation mechanisms. Per NUREG-0691 (Reference 2-2), a study on pipe cracking in PWR piping reported only two incidents of wall thinning in stainless steel pipe and these were not in the surge line. The cause of wall thinning is related to the high water velocity and is therefore clearly not a mechanism that would affect the surge line.

A known condition is the pressurizer surge line being subjected to thermal stratification; the effects of stratification are particularly significant during certain modes of operation. The effects of stratification have been evaluated for the Waterford 3 surge line and the loads, accounting for the stratification effects, have been derived. These loads are used in the Leak-Before-Break evaluation described in this report.

The Waterford 3 surge line piping system is fabricated from Cast Austenitic Stainless Steel (CASS) material (see Section 4.0) which is susceptible to toughness degradation due to thermal aging. The effect of thermal material aging degradation is considered (see Section 4.0) in the LBB analysis.

Finally, the maximum operating temperature of the Pressurizer surge line piping, which is about 650°F, is well below the temperature that would cause significant mechanical creep damage in stainless steel piping. Cleavage type failures are not a concern for the operating temperatures and the material used in the stainless steel piping of the Pressurizer surge line.

2.5 REFERENCES

- 2-1 Investigation and Evaluation of Stress-Corrosion Cracking in Piping of Light Water Reactor Plants, NUREG-0531, U.S. Nuclear Regulatory Commission, February 1979.
- 2-2 Investigation and Evaluation of Cracking Incidents in Piping in Pressurized Water Reactors, NUREG-0691, U.S. Nuclear Regulatory Commission, September 1980.

3.0 LOADS FOR FRACTURE MECHANICS ANALYSIS

3.1 NATURE OF THE LOADS

Figure 3-1 shows a schematic layout of the surge line for Waterford 3 and identifies the weld locations by Node point used in the LBB analysis. Although there are numerous other weld locations in the surge line, only selected weld locations were chosen based on the magnitude of the moments and on the proximity of a given location to an elbow, since piping elbows exhibit the greatest stress intensification. In general, the most highly stressed locations are in the vicinity of the elbows at either end of the surge line. Therefore, Nodes 70, 75, 80, 10, 20, and 25 were selected for LBB analysis. Additionally, intermediate locations that coincide with piping elbows and pipe whip restraints of interest (i.e., Nodes 45 and 55) were also selected for LBB analysis.

The stresses due to axial loads and resultant moments were calculated by the following equation:

$$\sigma = \frac{F}{A} + \frac{M}{Z} \quad (3-1)$$

where,

σ	=	Stress
F	=	Axial Load
M	=	Resultant Moment
A	=	Component Cross-Sectional Area
Z	=	Section Modulus

The moments for the desired loading combinations were calculated by the following equation:

$$M = (M_x^2 + M_y^2 + M_z^2)^{0.5} \quad (3-2)$$

where,

x axis is along the center line of the pipe.

M	=	Resultant Moment for Required Loading
M_x	=	Torsional Moment
M_y	=	Y Component of Bending Moment
M_z	=	Z Component of Bending Moment

The axial load and resultant moments for crack stability analysis and leak rate predictions are computed by the methods explained in Sections 3.2 and 3.3. Table 3-1 shows the dimensions used in the LBB analysis.

3.2 LOADS FOR CRACK STABILITY ANALYSIS

In accordance with SRP 3.6.3 (Reference 3-1) the absolute sum of loading components can be applied which results in higher magnitude of combined loads. If crack stability is demonstrated using these loads, the LBB margin can be reduced from $\sqrt{2}$ to 1.0. The faulted loads for the crack stability analysis were calculated by the absolute sum method as follows:

$$F = |F_{DW}| + |F_{TH}| + |F_P| + |F_{SSE}| \quad (3-3)$$

$$M_x = |M_{x,DW}| + |M_{x,TH}| + |M_{x,SSE}| \quad (3-4)$$

$$M_y = |M_{y,DW}| + |M_{y,TH}| + |M_{y,SSE}| \quad (3-5)$$

$$M_z = |M_{z,DW}| + |M_{z,TH}| + |M_{z,SSE}| \quad (3-6)$$

where

DW = Deadweight

TH = Applicable Thermal Expansion Load (Normal or Stratified)

P = Load Due to Internal Pressure

SSE = Safe Shutdown Earthquake Loading Including Seismic Anchor Motion

Note: various loadings for the surge line evaluation are identified in Table 3-2. The effects from fluid momentum are negligible due to the low flow rates in the surge line and these effects are ignored for the analysis.

3.3 LOADS FOR LEAK RATE EVALUATION

The normal operating loads for leak rate predictions were calculated by the algebraic sum method as follows:

$$F = F_{DW} + F_{TH} + F_P \quad (3-7)$$

$$M_x = M_{x,DW} + M_{x,TH} \quad (3-8)$$

$$M_y = M_{y,DW} + M_{y,TH} \quad (3-9)$$

$$M_z = M_{z,DW} + M_{z,TH} \quad (3-10)$$

The parameters and subscripts are the same as those explained in Sections 3.1 and 3.2.

Note: various loading for the surge line evaluation are identified in Table 3-2.

3.4 LOADING CONDITIONS

Because thermal stratification in the surge line is a recognized condition (Reference 3-4) and can cause large piping stresses, a review of the stratification stresses was performed to identify the upper bound loadings. The loading states so identified are given in Table 3-2. Applied loads on the surge line piping system are obtained from Waterford 3 uprate pipe stress reanalysis. Five different loads from the pipe stress analyses are considered in the LBB evaluation: dead-weight, normal operation (NOP) at 100% power thermal, normal operation stratification, maximum (high) stratification, and safe shutdown earthquake (SSE). Pressure loads are calculated separately and are included in the LBB evaluation.

Seven loading cases were identified and are shown in Table 3-3. Cases A, B, C are the normal operating load cases and Cases D, E, F and G are the faulted load cases. The cases of primary interest are the postulation of a detectable leak at normal 100% power [

] ^{a,c,e}

Case Combination [

] ^{a,c,e}

The case combination [

] ^{a,c,e}

[

] ^{a,c,e}

The realistic cases [

^{a,c,e} Table 3-4 shows the LBB analysis combination cases.

The RCS fluid was assumed to be completely stratified only in the horizontal run of the surge line piping. [

^{a,c,e} and the NOP pressure of 2,250 psia was used.

3.5 SUMMARY OF LOADS

The combined loads were evaluated at the various weld locations. Normal loads were determined using the algebraic sum method whereas faulted loads were combined using the absolute sum method. Table 3-5 shows loads and stresses at the three highest stressed weld locations. For the entire surge line, the highest stress ratio between loading Cases A or B and loading Case F falls within these weld locations. The minimum pipe wall thickness was used in the analysis. Lower normal loads govern for the leak rate calculation since lower loads will yield larger leakage flaw size. Higher faulted loads govern for the stability calculation since higher loads will yield smaller critical flaw size and J-integral results. By reviewing the various loading cases it is determined that the governing normal loading is Case A and governing faulted is Case F. Case A/F provides the overall governing flaw size margin. Therefore, fracture mechanics LBB analyses (leak rate and stability) are performed using the Case A and Case F loads at the critical locations. Table 3-6 shows the loads and stresses at the governing Alloy 82/182 welds location.

3.6 GOVERNING LOCATIONS

Node 70 is the highest stress weld location in the Waterford 3 surge line and this is the most critical location. The second and third highest stress locations are at Node 75 and Node 20 respectively. LBB analyses were performed at these three weld locations along the surge line. The weld processes used at these locations are GTAW/SMAW combinations.

For the two weld overlay nozzle locations at the ends of the surge line, the hot leg to surge line nozzle (Node 10) has the highest stresses and therefore is the critical SWOL location. Figure 3-1 shows the weld locations analyzed as identified by the Node numbers.

3.7 REFERENCES

- 3-1 NUREG-0800 Revision 1, March 2007, Standard Review Plan: 3.6.3 Leak-Before-Break Evaluation Procedures.
- 3-2 Materials Reliability Program: Leak-Before-Break Evaluation for PWR Alloy 82/182 Welds (MRP-140). EPRI, 1011808, November 2005.
- 3-3 Materials Reliability Program: Advanced FEA Evaluation of Growth of Postulated Circumferential PWSCC Flaws in Pressurizer Nozzle Dissimilar Metal Welds (MRP-216, Rev. 1): Evaluations Specific to Nine Subject Plants. EPRI, Palo Alto, CA, 1015400, August 2007.
- 3-4 NRC Bulletin No. 88-11. "Pressurizer Surge Line Thermal Stratification." December 20, 1988.

Table 3-1 Critical Location Dimensions (inches)			
Node (Location)	Outside Diameter	Inside Diameter	Minimum Thickness
Hot Leg to Surge Line Nozzle (Node 10)	14.59 (includes SWOL)	10.125	2.233 (includes SWOL)
	12.98 (without SWOL)		1.4275 (without SWOL)
Intermediary Surge Line Locations (Nodes 20, 70, 75)	12.750	10.413	1.1685

Table 3-2 Types of Loadings	
Pressure (P)	
Dead Weight (DW)	
Normal Operating Thermal Expansion (TH)	
Safe Shutdown Earthquake including Seismic Anchor Motion (SSE)	
[] ^{a,c,e}
[] ^{a,c,e}

Table 3-3 Normal and Faulted Loading Cases for Leak-Before-Break Evaluations	
Case A	Normal operating case at 653°F consisting of the algebraic sum of the loading components due to P, DW and TH.
Case B	[] ^{a,c,e}
Case C *	[] ^{a,c,e}
Case D	Faulted operating case at 653°F consisting of the absolute sum of P, DW, TH, and SSE
Case E	[] ^{a,c,e}
Case F	Faulted loads case with [] ^{a,c,e} stratification [] ^{a,c,e}
Case G *	[] ^{a,c,e}

* Case C and Case G are shown for information only

Note:

All thermal conditions analyzed included all of the applicable thermal loads and boundary conditions, including axial thermal expansion loads as well as any coincident thermal stratification loads.

A/D	This is the standard Leak-Before-Break evaluation.
A/F	This depicts a case with a detectable leak [] a,c,e
B/E	[] a,c,e
B/F	This depicts a detectable leak [] a,c,e

Table 3-5 Summary of Loads and Stresses at the Critical Locations				
Node Point	Load Case	Axial Force F (lbs)	Moment M (in-lbs)	Total Stress (ksi)
Node 70	A	176,856	732,814	10.65
	B	176,712	876,529	11.92
	C*	169,632	2731,126	28.17
	D	206,202	911,250	12.92
	E	206,346	1088,145	14.49
	F	211,140	2851,704	30.21
	G*	213,426	2957,130	31.20
Node 75	A	189,227	719,084	10.82
	B	189,431	773,639	11.30
	C*	190,673	2433,885	26.03
	D	194,819	893,058	12.49
	E	195,023	1023,346	13.65
	F	195,519	2627,186	27.86
	G*	196,265	2746,492	28.93
Node 20	A	187,241	749,973	11.04
	B	187,219	777,581	11.29
	C*	191,737	2268,053	24.59
	D	194,409	990,291	13.34
	E	194,431	1063,081	13.98
	F	195,447	2416,016	25.99
	G*	196,427	2604,609	27.68

*For information only.

Location	Load Case	Axial Force F (lbs)	Moment M (in-lbs)	Total Stress (ksi)
Hot Leg to Surge Line Nozzle (Node 10)	A	176,607	761,720	5.29
	B	176,585	849,370	5.66
	[] ^{a,c,e}

[

] ^{a,c,e}

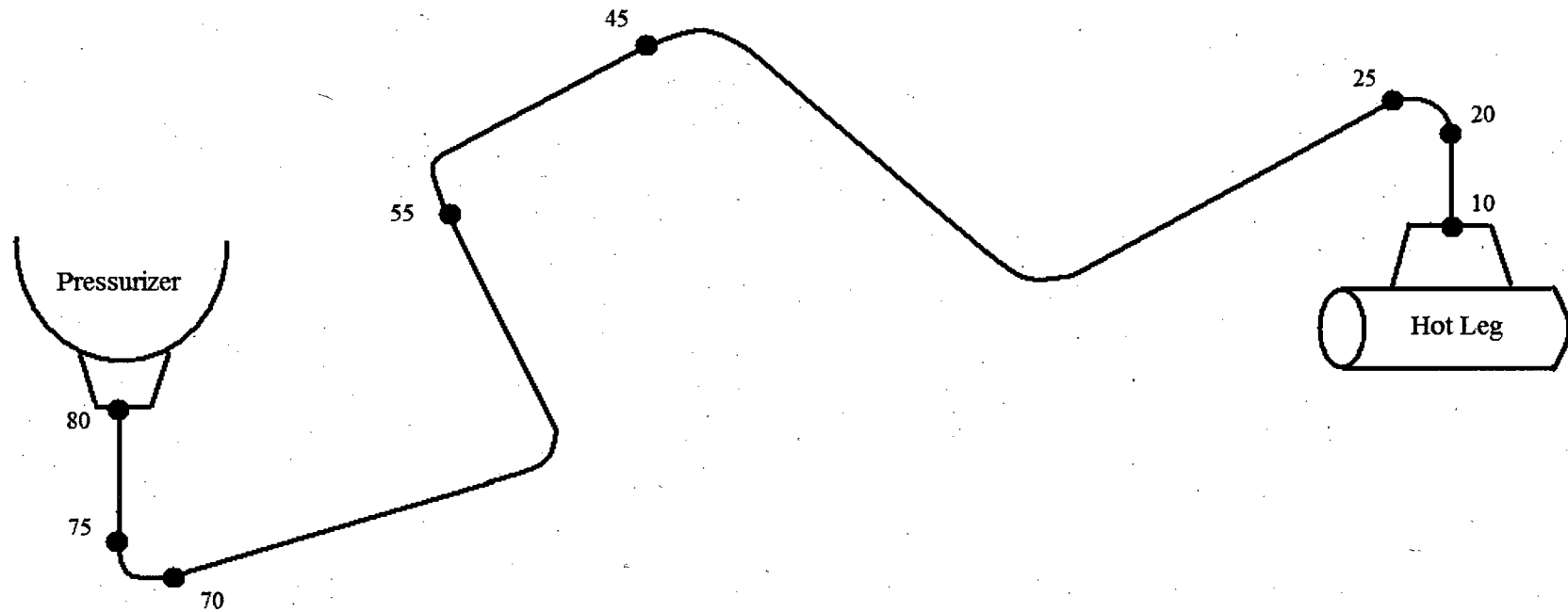


Figure 3-1 Schematic Layout of Waterford 3 Surge Line Showing LBB Analyzed Weld Location by Nodes

4.0 MATERIAL CHARACTERIZATION

4.1 PIPE MATERIAL AND WELDING PROCESS

The Waterford 3 surge line piping system is fabricated from Schedule 160 pipe made of cast austenitic stainless steel (CASS) SA-351 CF8M material. The piping system connects at one end to the hot leg surge nozzle and at the other end to the Pressurizer surge nozzle through CASS SA-351 safe-ends.

The weld processes used to fabricate the surge line are a combination of Gas Tungsten Arc Welding (GTAW) and Shielded Metal Arc Welding (SMAW). The safe-ends are welded to the hot leg surge nozzle and Pressurizer surge nozzle with Alloy 82/182 welds. Alloy 82/182 welds have been mitigated by structural weld overlays (SWOLs) using Alloy 52M weld material. Currently, both ends of the surge line have a composite geometry consisting of the original design Alloy 82/182 weld dimensions overlaid with 52M material.

Figure 3-1 shows the schematic layout of the surge line and identifies the weld locations by Node points. Node 10 represents the piping to hot leg nozzle interface, while Node 80 represents the piping to Pressurizer nozzle interface.

In the following sections the tensile properties and fracture mechanics properties of the materials are presented which were used in the leak-before-break analyses.

4.2 MATERIAL PROPERTIES

4.2.1 Tensile Material Properties

Tensile properties and chemical compositions for the CASS base material on the Waterford 3 surge line were obtained from the certified material test reports (CMTRs). CMTR mechanical properties correspond to a specific heat of material from empirically tested values. The representative properties of the material heat at operating temperatures were established from the tensile properties at room temperature by utilizing the ASME Code 1971 Edition through Winter Addendum, Section II, Part A (Reference 4-1). Code tensile properties at the required operating temperatures were obtained by interpolating between the room temperature and higher temperature tensile properties. Ratios of the ASME Code tensile properties at operating temperature to the corresponding properties at room temperature were then applied to the room temperature tensile properties obtained from CMTRs to obtain the Waterford 3 specific properties at operating temperatures. Table 4-1 shows the tensile properties for the SA-351 CF8M base material.

Mechanical properties for the stainless steel weld material at ambient temperature were obtained from the Battelle database (Reference 4-2). The representative properties at operating temperatures were established from the tensile properties at room temperature by utilizing the ASME Code 1971 Edition through Winter Addendum, Section II, Part A (Reference 4-1). Code tensile properties at the required operating temperatures were obtained by interpolating between the room temperature and higher temperature tensile properties. Ratios of the ASME

Code tensile properties at operating temperature to the corresponding properties at room temperature were then applied to the room temperature tensile properties obtained from the database to obtain the Waterford 3 specific properties at operating temperatures. Table 4-1 shows the tensile properties for the stainless steel weld material.

The representative Alloy 82/182 and Alloy 52M weld metals properties, as shown in Table 4-2, were based on industry data compiled by Westinghouse for the weld overlay application and used here for LBB application.

The ASME Code modulus of elasticity values are obtained from (Reference 4-3). The Poisson's ratio was taken as 0.30. Mechanical properties from Table 4-1 and Table 4-2 were used for the LBB fracture mechanics analyses.

4.2.2 Fracture Toughness Material Properties

Cast stainless steel is susceptible to thermal aging during service. Thermal aging of cast stainless steel results in a decrease in the ductility, impact strength, and fracture toughness, of the material. Depending on the material composition, the Charpy impact energy of a cast stainless steel component could decrease to a small fraction of its original value after exposure to reactor temperatures during service. Alloy 82/182 and Alloy 52M welds do not exhibit thermal aging degradation like cast stainless steel does.

In 1994, the Argonne National Laboratory (ANL) completed an extensive research program in assessing the extent of thermal aging of cast stainless steel materials. The ANL research program measured mechanical properties of cast stainless steel materials after they have been heated in controlled ovens for long periods of time. ANL compiled a database, both from data within ANL and from international sources, of about 85 compositions of cast stainless steel exposed to a temperature range of 290-400°C (550-750°F) for up to 58,000 hours (6.5 years). From this database, ANL developed correlations for estimating the extent of thermal aging of cast stainless steel (References 4-4 and 4-5).

ANL developed the fracture toughness estimation procedures by correlating data in the database conservatively. After developing the correlations, ANL validated the estimation procedures by comparing the estimated fracture toughness with the measured value for several cast stainless steel plant components removed from actual plant service. The ANL procedures produced conservative estimates that were about 30 to 50 percent less than actual measured values. The procedure developed by ANL in Reference 4-5 was used to calculate the end of life fracture toughness values for this analysis. ANL research program was sponsored and the procedure was accepted (Reference 4-6) by the NRC.

The following equations are taken from Reference 4-5:

$$Cr_{eq} = Cr + 1.21(Mo) + 0.48(Si) - 4.99 \quad (4-1)$$

$$Ni_{eq} = (Ni) + 0.11(Mn) - 0.0086(Mn)^2 + 18.4(N) + 24.5(C) + 2.77 \quad (4-2)$$

where Cr_{eq} = (Chromium equivalent); Ni_{eq} =(nickel equivalent);

δ_c (ferrite content) in percent volume is given by:

$$\delta_c = 100.3(Cr_{eq} / Ni_{eq})^2 - 170.72(Cr_{eq} / Ni_{eq}) + 74.22 \quad (4-3)$$

The saturation room temperature (RT) impact energies of the cast stainless steel materials were determined from the chemical compositions.

For CF8M steel with < 10% Ni, the saturation value of RT impact energy Cv_{sat} (J/cm²) is the lower value determined from

$$\log_{10} Cv_{sat} = 1.10 + 2.12 \exp(-0.041\phi) \quad (4-4)$$

where the material parameter ϕ is expressed as

$$\phi = \delta_c (Ni + Si + Mn)^2 (C + 0.4N) / 5.0 \quad (4-5)$$

and from

$$\log_{10} Cv_{sat} = 7.28 - 0.011\delta_c - 0.185Cr - 0.369Mo - 0.451Si - 0.007Ni - 4.71(C + 0.4N) \quad (4-6)$$

For CF8M steel with > 10% Ni, the saturation value of RT impact energy Cv_{sat} (J/cm²) is the lower value determined from

$$\log_{10} Cv_{sat} = 1.10 + 2.64 \exp(-0.064\phi) \quad (4-7)$$

where the material parameter ϕ is expressed as

$$\phi = \delta_c (Ni + Si + Mn)^2 (C + 0.4N) / 5.0 \quad (4-8)$$

and from

$$\log_{10} Cv_{sat} = 7.28 - 0.011\delta_c - 0.185Cr - 0.369Mo - 0.451Si - 0.007Ni - 4.71(C + 0.4N) \quad (4-9)$$

The saturation J-R curve at RT, for static-cast CF8M steel is given by

$$J_d = 16(Cv_{sat})^{0.67} (\Delta a)^n \quad (4-10)$$

and for centrifugally cast CF8M steel, by

$$J_d = 20(Cv_{sat})^{0.67} (\Delta a)^n \quad (4-11)$$

where the exponent n for CF8M steel is expressed as

$$n = 0.23 + 0.08 \log_{10} (Cv_{sat}) \quad (4-12)$$

where J_d is the "deformation J" in kJ/m² and Δa is the crack extension in mm.

The saturation J-R curve at 290°C (554°F), for static-cast CF8M steel is given by

$$J_d = 49 (Cv_{sat})^{0.41} (\Delta a)^n \quad (4-13)$$

and for centrifugally cast CF8M steel, by

$$J_d = 57 (Cv_{sat})^{0.41} (\Delta a)^n \quad (4-14)$$

where the exponent n for CF8M steel is expressed as

$$n = 0.23 + 0.06 \log_{10} (Cv_{\text{sat}}) \quad (4-15)$$

where J_d is the "deformation J" in kJ/m^2 and Δa is the crack extension in mm.

Tensile properties are used for the crack stability J-integral analysis in Section 6.0.

For the CASS base material, the J-resistance parameters for all the surge line component materials are determined by

$$J_d = \beta(\Delta a)^m \quad (4-16)$$

where

J_d is the fracture toughness, in.-lb/in.^2 ,

Δa is the crack extension, in.,

β is the constant, $(\text{in.-lb/in.}^2)/\text{in.}^m$, and

m is the exponent (Note: " m " corresponds to " n " in the Equations 4-10 to 4-15).

In the case of the saturation values with unknown thermal aging service history, CF8M material chemistry was used to derive β and m at locations along the pipeline. Table 4-4 shows the J_R (J-resistance) curve parameters at all locations for the surge line. A lower bound value for the surge line occurs for piece number 751-110 of assembly number 751-107, a fabricated component of 12" schedule 160 x 75 degrees, long radius elbow. The chemistry of this critical heat based on CMTR is given in Table 4-3. Procedures outlined in (Reference 4-5) were employed in deriving the J-resistance property from the CMTR chemistry for CF8M material. The J_{Ic} and J_{max} at the CASS base metal and stainless steel weld metal at various node locations are shown in Table 4-5.

[

]a,c,e

In the fracture mechanics analyses that follow, the fracture toughness properties given in Table 4-5 will be used as the criteria against which the applied fracture toughness values will be compared.

4.3 REFERENCES

- 4-1 ASME Boiler and Pressure Vessel Code, Section II, Part A, 1971 Edition through Winter Addendum.
- 4-2 US NRC Battelle Database, "Pipe Fracture Encyclopedia," Volume 1, 1997.
- 4-3 ASME Boiler and Pressure Vessel Code, 1971 Edition, Section III, Appendix I.
- 4-4 O. K. Chopra and W. J. Shack, "Assessment of Thermal Embrittlement of Cast Stainless Steels," NUREG/CR-6177, U. S. Nuclear Regulatory Commission, Washington, DC, May 1994.
- 4-5 O. K. Chopra, "Estimation of Fracture Toughness of Cast Stainless Steels during Thermal Aging in LWR Systems," NUREG/CR-4513, Revision 1, U. S. Nuclear Regulatory Commission, Washington, DC, August 1994.
- 4-6 "Flaw Evaluation of Thermally Aged Cast Stainless Steel in Light-Water Reactor Applications," Lee, S.; Kuo, P. T.; Wichman, K.; Chopra, O.; Published in International Journal of Pressure Vessel and Piping, June 1997.

Table 4-1 Tensile Material Properties for Cast Stainless Steel Base and Stainless Steel Weld Metal at the Critical Locations			
Node (Temperature)	Yield Strength (ksi)	Ultimate Strength (ksi)	Modulus of Elasticity (ksi)
Nodes 20, 70, 75 Base Metal** (653°F)	29.41	82.46	25.08 x 10 ³
Node 70 Base Metal** [] ^{a,c,e}	30.15	82.46	25.43 x 10 ³
Nodes 20, 70, 75 Stainless Steel Weld Metal (653°F)	33.63	76.51	25.03 x 10 ³
Node 70 Stainless Steel Weld Metal [] ^{a,c,e}	34.50	76.51	25.32 x 10 ³
Node 20 Base Metal [] ^{a,c,e}	37.52	83.77	26.97 x 10 ³
Node 20 Stainless Steel Weld Metal [] ^{a,c,e}	42.89	81.40	26.81 x 10 ³

**Base Metal at Nodes 20, 70, 75 is cast austenitic stainless steel

Table 4-2 Tensile Material Properties for Alloy 82/182 and Alloy 52M at the Critical SWOL Location (Node 10)			

a,c,e

Element	Chemical Composition (%)
Carbon	0.06
Manganese	0.57
Silicone	0.99
Chromium	20.66
Nickel	9.06
Molybdenum	2.51

Table 4-5 Fracture Toughness Properties used to Evaluate Critical Locations at Cast Austenitic Stainless Steel Surge Line

Location	Material	J _{IC} (in-lb/in ²)	T _{mat} (non-dimensional)	J _{max} (in-lb/in ²)

a,c,e

5.0 LEAK RATE PREDICTIONS

5.1 INTRODUCTION

The purpose of this section is to discuss the method which is used to predict the flow through postulated through-wall cracks and present the leak rate calculation results for through-wall circumferential cracks.

Fracture mechanics analysis shows that postulated through-wall cracks in the surge line would remain stable (Section 6.0) and would not cause a gross failure of this component. However, if such a through-wall crack did exist, it would be desirable to detect the leakage such that the plant could be brought to a safe shutdown condition. The purpose of this section is to discuss the method that will be used to predict the flow through such a postulated crack and present the leak rate calculation results for through-wall circumferential cracks.

5.2 GENERAL CONSIDERATIONS

The flow of hot pressurized water through an opening to a lower backpressure (causing choking) is taken into account. For long channels where the ratio of the channel length, L , to hydraulic diameter, D_H , (L/D_H) is greater than $[]^{a,c,e}$ both $[]^{a,c,e}$ must be considered. In this situation, the flow can be described as being single-phase through the channel until the local pressure equals the saturation pressure of the fluid. At this point, the flow begins to flash and choking occurs. Pressure losses due to momentum changes will dominate for $[]^{a,c,e}$. However, for large L/D_H values, the friction pressure drop will become important and must be considered along with the momentum losses due to flashing.

5.3 CALCULATION METHOD

In using the $[]^{a,c,e}$

The flow rate through a crack was calculated in the following manner. Figure 5-1 from Reference 5-2 was used to estimate the critical pressure, P_c , for the primary loop enthalpy condition and an assumed flow. Once P_c was found for a given mass flow, the $[]^{a,c,e}$

$[]^{a,c,e}$ was found from Figure 5-2 taken from Reference 5-2. For all cases considered, since $[]^{a,c,e}$

$[]^{a,c,e}$ Therefore, this method will yield the two-phase pressure drop due to momentum effects as illustrated in Figure 5-3. Now using the assumed flow rate, G , the frictional pressure drop can be calculated using

$$\Delta P_f = []^{a,c,e} \quad (5-1)$$

where the friction factor f was determined using the []^{a,c,e}. The crack relative roughness, ε , was obtained from fatigue crack data on stainless steel samples. The relative roughness value used in these calculations was []^{a,c,e} RMS.

The frictional pressure drop using Equation 5-1 was then calculated for the assumed flow and added to the []^{a,c,e} to obtain the total pressure drop from the system under consideration to the atmosphere. Thus,

$$\text{Absolute Pressure} - 14.7 = []^{\text{a,c,e}} \quad (5-2)$$

for a given assumed flow G . If the right-hand side of Equation 5-2 does not agree with the pressure difference between the piping under consideration and the atmosphere, then the procedure is repeated (iterated) until Equation 5-2 is satisfied to within an acceptable tolerance and results in the flow value through the crack.

5.4 LEAK RATE CALCULATIONS

Leak rate calculations were performed as a function of postulated through-wall crack length for the critical locations previously identified. The crack opening area was estimated using the method of Reference 5-3 and the leak rates were calculated using the calculation methods described above. The leak rates were calculated using the normal operating loads at the governing locations identified in Section 3.0.

For the surge line piping critical locations, yield strength properties shown in Table 4-1 were used for the leak rate calculation. The crack lengths yielding a leak rate of 2.5 gpm (10 times the leak detection capability of 0.25 gpm) for the critical locations in the Waterford 3 Pressurizer surge line piping are shown in Table 5-1.

[

face

5.5 REFERENCES

- 5-1 []^{a,c,e}
- 5-2 M. M, El-Wakil, "Nuclear Heat Transport, International Textbook Company," New York, N.Y, 1971.
- 5-3 Tada, H., "The Effects of Shell Corrections on Stress Intensity Factors and the Crack Opening Area of Circumferential and a Longitudinal Through-Crack in a Pipe," Section II-1, NUREG/CR-3464, September 1983.
- 5-4 Rahman, S., Ghadiali, N., Paul, D., and Wilkowski, G., "Probabilistic Pipe Fracture Evaluations for the Leak-Rate-Detection Applications," NUREG/CR-6004, BMI-2174, April 1995.
- 5-5 Nana, A. D., Yoon, K. K., PVP2006-ICPVT11-93767, July 23-27, 2006, Vancouver, Canada, "Comparison of Leak Rates from Alloy 82/182 Butt Weld Cracks for Leak-Before-Break Applications."
- 5-6 Rudland, D. L., Wolterman, R., Wilkowski G., and Tregoning, R., "Impact of PWSCC and Current Leak Detection on Leak-Before-Break," Proceedings of Conference on Vessel Head Penetration Inspection, Cracking, and Repairs, Sponsored by USNRC, Marriot Washingtonian Center, Gaithersburg, MD, September 29 to October 2, 2003.

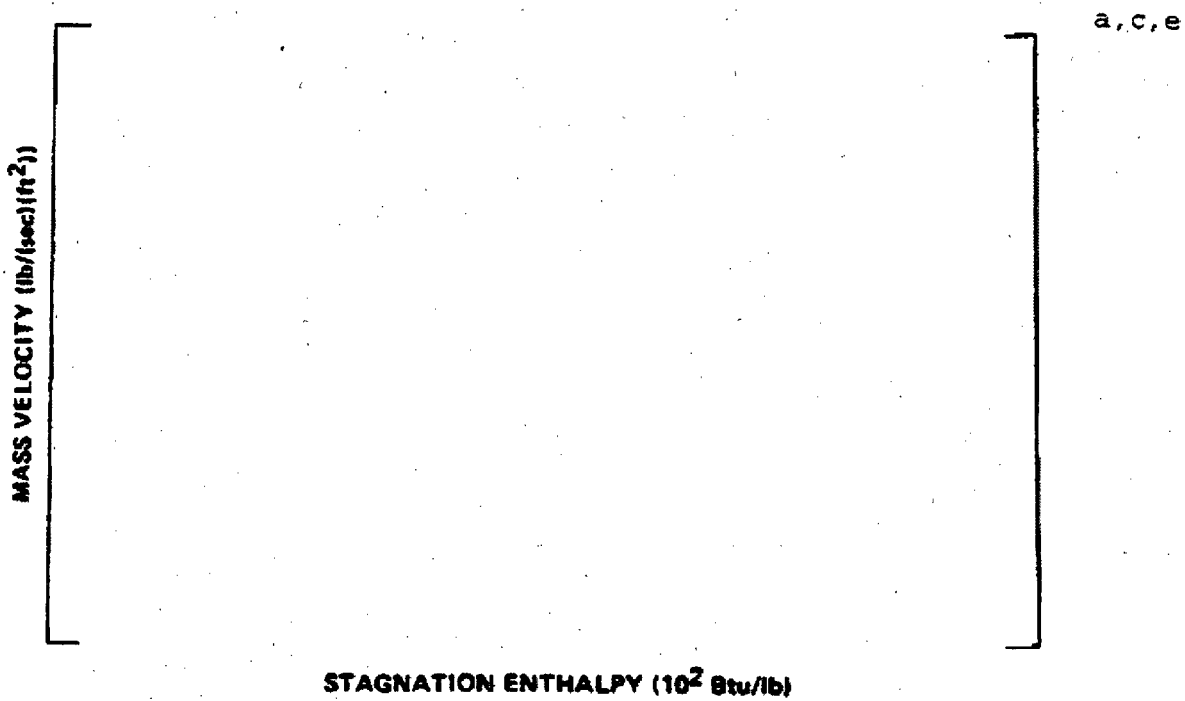


Figure 5-1 Analytical Predictions of Critical Flow Rates of Steam-Water Mixtures

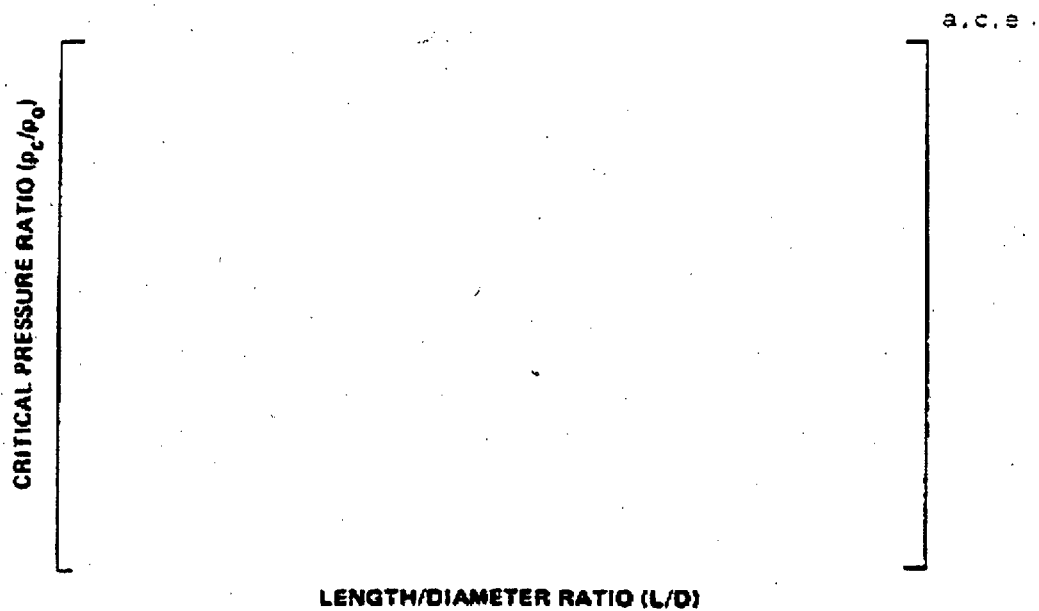


Figure 5-2 [

] ^{a,c,e} Pressure Ratio as a Function of L/D

Node Location	Material	Leakage Flaw (in.)
70	Base Metal	3.18
	Weld Metal	3.24
75	Base Metal	3.14
	Weld Metal	3.20
20	Base Metal	3.10
	Weld Metal	3.16

The governing loading case is Case A.

Node Location	Material	Leakage Flaw (in.)

a, c, e

6.0 FRACTURE MECHANICS EVALUATION

6.1 LOCAL FAILURE MECHANISM

The local mechanism of failure is primarily dominated by the crack tip behavior in terms of crack-tip blunting, initiation, extension and final crack instability. The local stability will be assumed if the crack does not initiate at all. It has been accepted that the initiation toughness measured in terms of J_{Ic} from a J-integral resistance curve is a material parameter defining the crack initiation. If, for a given load, the calculated J-integral value is shown to be less than the J_{Ic} of the material, then the crack will not initiate. If the initiation criterion is not met, one can calculate the tearing modulus (see Equation A-14a of Reference 6-1) as defined by the following relation:

$$T_{app} = \frac{dJ}{da} \times \frac{E}{\sigma_f^2} \quad (6-1)$$

where:

- T_{app} = applied tearing modulus
- E = modulus of elasticity
- [$J_{a,c,e}$]
- a = crack length
- σ_y, σ_u = yield and ultimate strength of the material, respectively

Stability is said to exist when ductile tearing does not occur if T_{app} is less than T_{mat} , the experimentally determined tearing modulus. Since a constant T_{mat} is assumed a further restriction is placed in J_{app} . J_{app} must be less than J_{max} where J_{max} is the maximum value of J for which the experimental T_{mat} is greater than or equal to the T_{app} used.

Fracture mechanics analyses are made based on loads and postulated flaw sizes related to leakage. The stability criteria against which the calculated J and tearing modulus are compared are:

- (1) If $J_{app} < J_{Ic}$, then the crack will not initiate and the crack is stable;
- (2) If $J_{app} \geq J_{Ic}$, then the crack is stable only if both $T_{app} < T_{mat}$ and $J_{app} < J_{max}$ are satisfied

Where:

J_{app}	=	Applied J
J_{Ic}	=	J at Crack Initiation
T_{app}	=	Applied Tearing Modulus
T_{mat}	=	Material Tearing Modulus
J_{max}	=	Maximum J value of the material

For the critical locations, the limit load method discussed in Section 6.2 was also used.

6.2 GLOBAL FAILURE MECHANISM

Determination of the conditions that lead to failure in stainless steel should be done with plastic fracture methodology because of the large amount of deformation accompanying fracture. One method for predicting the failure of ductile material is the []^{a,c,e} method based on traditional plastic limit load concepts, but accounting for []^{a,c,e} and taking into account the presence of a flaw. The flawed component is predicted to fail when the remaining net section reaches a stress level at which a plastic hinge is formed. The stress level at which this occurs is termed as the flow stress. The flow stress is generally taken as the [

] ^{a,c,e} at the temperature of interest. This methodology has been shown to be applicable to ductile piping through a large number of experiments and is used here to predict the critical flaw size in the Pressurizer surge line. The failure criterion has been obtained by requiring equilibrium of the section containing the flaw (Figure 6-1) when loads are applied. The detailed development is provided in Appendix A for a through-wall circumferential flaw in a pipe section with internal pressure, axial force, and imposed bending moments. The limit moment for such a pipe is given by:

[

] a.c.e

The analytical model described above accurately accounts for the internal pressure as well as an imposed axial force as they affect the limit moment. Good agreement was found between the analytical predictions and the experimental results (Reference 6-2). Flaw stability evaluations, using this analytical model, are presented in Section 6.3.

6.3 STABILITY EVALUATION

6.3.1 Limit Moment Method

A typical segment of the pipe under maximum loads of axial force F and bending moment M is schematically illustrated in Figure 6-2. The critical flaw sizes for the stainless steel surge line locations are calculated using governing faulted loads from Table 3-5 and material properties from Table 4-1.

The welds at the stainless steel surge line governing locations are GTAW/SMAW combination. The "Z" factor for GTAW is 1.0 and therefore, the "Z" factor correction for the SMAW was applied (Reference 6-3) as follows:

$$Z = 1.15 [1 + 0.013 (OD - 4)] \text{ (for SMAW)} \quad (6-4)$$

where OD is the outer diameter in inches. Substituting $OD = 12.75$ inches, the "Z" factor was calculated to be 1.281 for SMAW. The applied loads were increased by the applicable Z factor and the plots of limit load versus crack length were generated for the governing cases with the lower critical flaw sizes as shown in Figures 6-3 to 6-5. Table 6-1 shows the summary of critical flaw sizes for the stainless surge line locations.

[

] a.c.e

6.3.2 J-integral Method

The Stability (J-integral) analyses were performed for the cases established previously in Section 6.1. The elastic-plastic fracture mechanics (EPFM) J-integral analyses for through-wall circumferential cracks in a cylinder were performed by using the EPRI Handbook procedures (Reference 6-4). The resulting J_{applied} and T_{applied} are listed in Table 6-3 and compared with the allowable fracture toughness values from Table 4-5. Allowable fracture toughness values are also shown in Table 6-3.

Based on the J-integral stability analysis results shown in Table 6-3, the stability criteria described in Section 6.1 are met. Therefore, it is concluded that the postulated circumferential through-wall flaws are stable and will not result in a full break of the pipe.

6.4 REFERENCES

- 6-1 NUREG-1061 Volume 3, "Report of the U. S. Nuclear Regulatory Commission Piping Review Committee," November 1984.
- 6-2 Kanninen, M. F. et al., "Mechanical Fracture Predictions for Sensitized Stainless Steel Piping with Circumferential Cracks" EPRI NP-192, September 1976.
- 6-3 NUREG-0800 Revision 1, March 2007, Standard Review Plan: 3.6.3 Leak-Before-Break Evaluation Procedures.
- 6-4 Kumar, V., German, M. D. and Shih, C. P., "An Engineering Approach for Elastic-Plastic Fracture Analysis," ERPI Report NP-1931, Project 1237-1, Electric Power Research Institute, July 1981.
- 6-5 ASME Pressure Vessel and Piping Division Conference Paper PVP2008-61840, "Technical Basis for Revision to Section XI Appendix C for Alloy 600/82/182/132 Flaw Evaluation in Both PWR and BWR Environments," July 28-31, 2008, Chicago IL, USA.

Table 6-1 Summary of Critical Flaw Size for Critical Locations			
Node Point	Faulted Load Case	Temperature (°F)	Critical Flaw Size (in)
70	F	[] ^{a,c,e}	10.5 ^a 10.4 ^b
75	F	[] ^{a,c,e}	11.2 ^a 11.1 ^b
20	F	[] ^{a,c,e}	12.6 ^a 12.8 ^b

^a Based on base metal tensile properties.

^b Based on weld metal tensile properties.

Table 6-2 Summary of Critical Flaw Size for SWOL Critical Location (Node 10)			
Location	Faulted Load Case	Temperature (°F)	Critical Flaw Size (in)

a,c,e

Table 6-3 Stability Results for Waterford 3 Pressurizer Surge Line Based on Elastic-Plastic J-integral Evaluations

Node	Flaw Size* (in)	Fracture Toughness Allowable Values			Calculated Values	
		J_{IC} (in-lb/in ²)	T_{mat}	J_{max} (in-lb/in ²)	J_{app} (in-lb/in ²)	T_{app}

a, c, e

Crack is stable if either of the two J-integral stability criteria below is met:

- (1) If $J_{app} < J_{IC}$, then the crack is stable
- (2) If $J_{app} \geq J_{IC}$, then the crack is stable only if both $T_{app} < T_{mat}$ and $J_{app} < J_{max}$ are satisfied

Therefore, for all the cases shown in Table 6-3 the stability criteria are met based on either of the two above conditions.

NA = Not Applicable. If $J_{app} < J_{IC}$, then it is not necessary to calculate T_{app} , since stability criteria (1) is met.

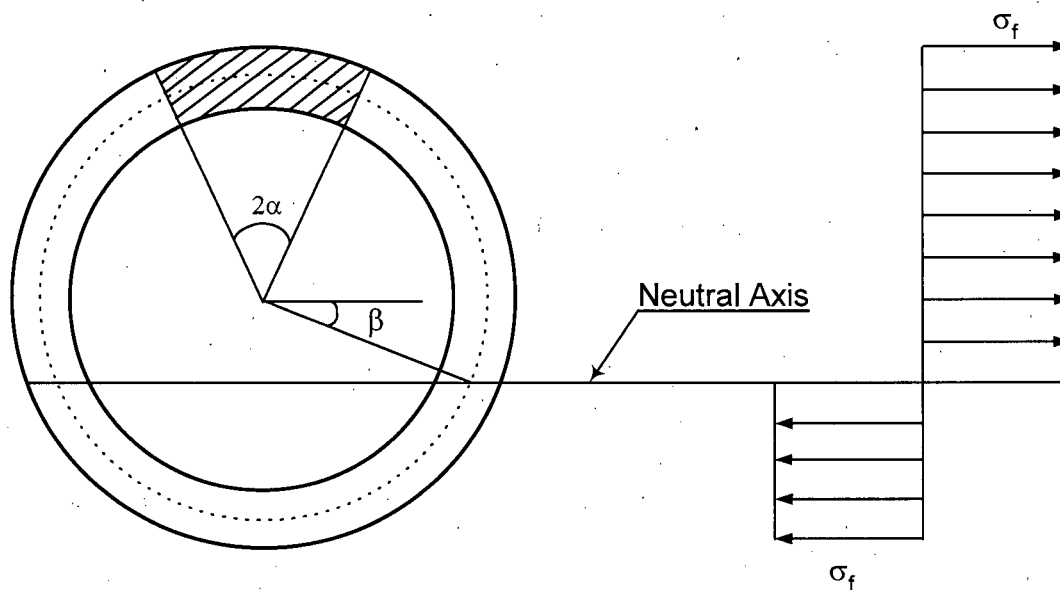


Figure 6-1 Fully Plastic Stress Distribution

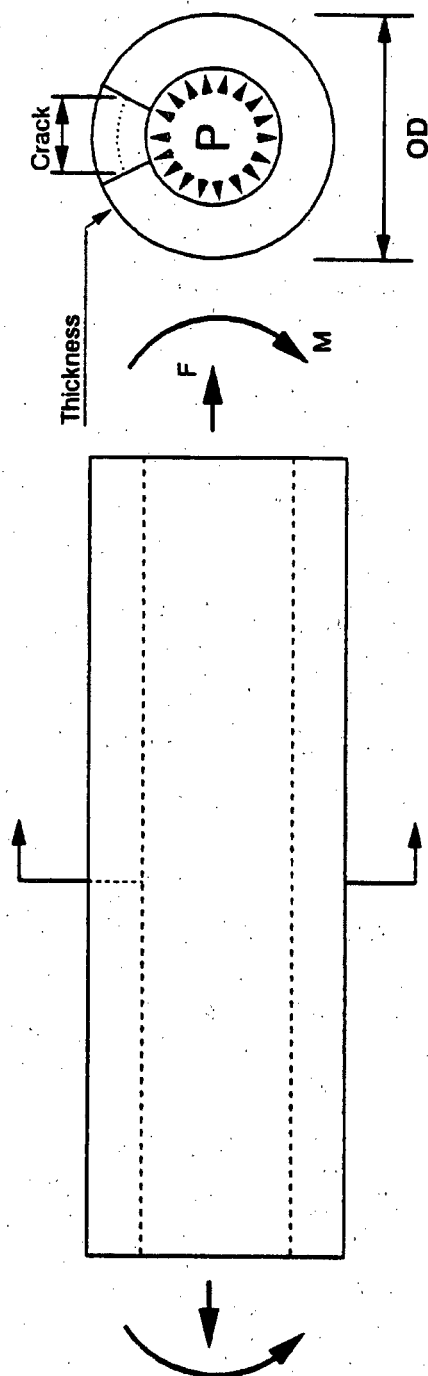


Figure 6-2 Loads Acting on the Model at the Governing Locations

a, c, e

OD = 12.75 in.	$\sigma_{y-min} = 34.50$ ksi	F = 211.140 kips
t = 1.168 in.	$\sigma_{u-min} = 76.51$ ksi	M = 2851.700 in-kips
SA-351 CF8M Weld Metal Faulted Case F		

Note: OD = outer diameter, t = thickness

Figure 6-3 Critical Flaw Size Prediction – Waterford 3 Node 70

a, c, e



OD = 12.75 in.	$\sigma_{y-min} = 33.63$ ksi	F = 195.519 kips
t = 1.168 in.	$\sigma_{u-min} = 76.51$ ksi	M = 2627.186 in-kips
SA-351 CF8M Weld Metal Faulted Case F		

Note: OD = outer diameter, t = thickness

Figure 6-4 Critical Flaw Size Prediction – Waterford 3 Node 75

a, c, e

OD = 12.75 in.	$\sigma_{y-min} = 37.52$ ksi	F = 195.447 kips
t = 1.168 in.	$\sigma_{u-min} = 83.77$ ksi	M = 2416.016 in-kips
SA-351 CF8M Base Metal Faulted Case F		

Note: OD = outer diameter, t = thickness

Figure 6-5 Critical Flaw Size Prediction – Waterford 3 Node 20

a, c, e

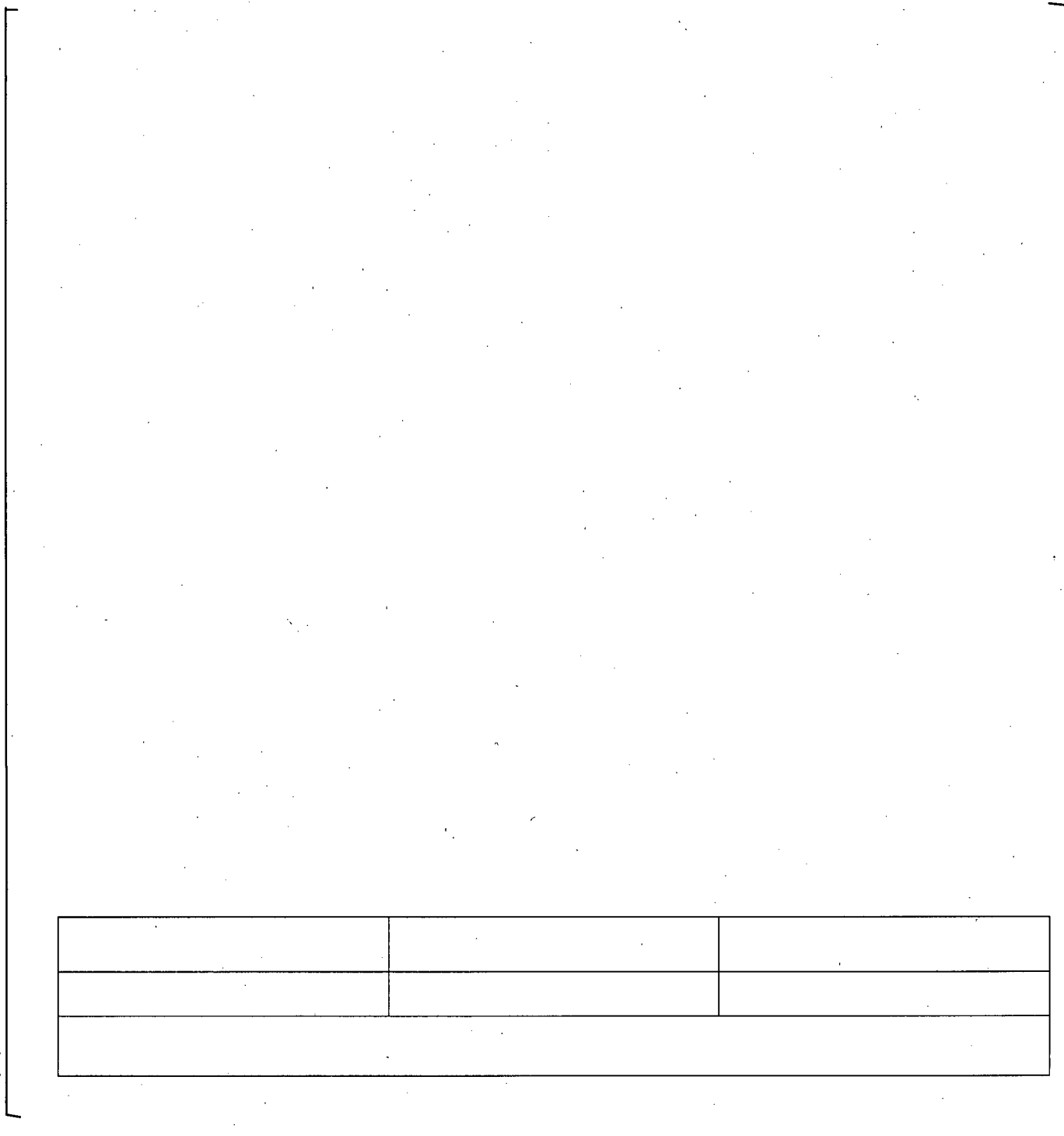


Figure 6-6 Critical Flaw Size Prediction – Waterford 3 Alloy 82/182 and Alloy 52M Welds

7.0 FATIGUE CRACK GROWTH ANALYSIS

The fatigue crack growth results at the dissimilar metal weld regions for the hot leg to surge line nozzle and pressurizer surge nozzle are analyzed by other (Reference 7-1) and presented here for completeness. The FCG results at an intermediate surge line location are analyzed by Westinghouse; Section 7.1 below describes the methodology used in determining the FCG for the stainless steel material at the intermediate surge line location. Results from both analyses are documented in Section 7.2.

7.1 METHODOLOGY

To determine the sensitivity of the Pressurizer surge line to the presence of postulated small cracks when subjected to the various transients, Fatigue Crack Growth (FCG) analyses were performed.

The methodologies consists of first obtaining the local and structural transient stress analyses results and then superimpose them to obtain the total stresses. The design cycles used in the FCG analyses are tabulated in Table 7-1. For the surge line piping, an initial flaw size was postulated and the calculation of the crack growth for the design plant life (40 years) using the austenitic stainless steel crack growth law was performed. The fatigue crack growth analysis was performed in the surge line pipe at an intermediate high stressed location (Node 70).

The reference fatigue crack growth curves for the stainless steel material in air environment from Appendix C of ASME Section XI is shown in Figure 7-1 (Reference 7-2). A compilation of data for austenitic stainless steel in a PWR water environment was made by Bamford (Reference 7-3), and it was found that the effect of the environment on the crack growth rate was small. For this reason it was conservatively estimated that the environmental factor should be set at []^{a,c,e} in the crack growth rate equation from Reference 7-4. Based on these works (References 7-3 and 7-4) the stainless steel fatigue crack growth law used in the analyses is:

$$\frac{da}{dN} = CS (\Delta K)^n F_{env} \quad (7-1)$$

where,

$$\frac{da}{dN} = \text{inches per cycle}$$

$$C = \text{material coefficient} = 10^{(-10.009+8.12E-4T-1.13E-06T^2+1.02E-09T^3)}$$

$$S = \begin{aligned} &1.0 \quad \text{for } R = 0; \\ &1 + 1.8R \quad \text{for } 0 < R \leq 0.79; \\ &-43.35 + 57.97R \quad \text{for } 0.79 < R < 1.0 \end{aligned}$$

$$n = \text{material property slope} = 3.30$$

ΔK = stress intensity factor range, ksi $\sqrt{\text{in}}$

F_{env} = environmental factor (= 1.0 for air environment, and = []^{a,c,e} for PWR environment)

7.2 FATIGUE CRACK GROWTH RESULTS

Pressurizer Surge Nozzle and Hot Leg to Surge Line Nozzle Welds

The Structural Weld Overlay FCG analysis at the Hot Leg to surge line nozzle and pressurizer nozzle dissimilar metal weld - DMW (nozzle-to-safe end weld) and the stainless steel weld - SSW (safe end-to-pipe weld) are performed in Reference 7-1. The analysis results are shown in Tables 7-2 and 7-3 for the pressurizer surge nozzle weld overlay regions and the hot leg to surge line nozzle weld overlay regions, respectively. Based on these results, it can be demonstrated that a continuous circumferential flaw that is 75% of the original weld thickness at the pressurizer surge nozzle weld overlay region (Table 7-2) would take 15 and 34 years for the DMW and SSW respectively to reach the weld overlay. At the hot leg to surge nozzle weld overlay region (Table 7-3), it was demonstrated that a continuous (around the entire circumference) circumferential flaw that is 75% of the original weld thickness would take more than 60 years for the DMW and 19 years for the SSW to reach the weld overlay. It can be noted that postulating an initial flaw size of 75% of the original weld thickness is very conservative.

Intermediate Stainless Steel Weld Location

The FCG results at an intermediate highest stressed surge line location are determined based on the transient information provided in Table 7-1. A circumferential flaw with an aspect ratio (flaw length/flaw depth) of 6.0 is analyzed with an initial depth of 10% of the wall thickness. The FCG is predicted based on a normal operating temperature of 653°F. Based on the analysis results, it was determined that a 10% circumferential through-the-wall flaw will only grow to 38% through the original wall thickness for the transients and cycles considered in Table 7-1.

Based on the FCG results shown in Table 7-4 of this report, it can be concluded that small postulated circumferential flaws will not propagate through the wall for the transients and cycles considered in Table 7-1.

7.3 REFERENCES

- 7-1 Entergy Letter, W3F1-2008-0037, "Summary of Design and Analyses of Weld Overlays for Pressurizer and Hot Leg Nozzle Dissimilar Metal Welds for Alloy 600 Mitigation Waterford Steam Electric Station, Unit 3 (Waterford 3)." Docket No. 50-382, License No. NPF-38. May 10, 2008.
- 7-2 ASME Boiler and Pressure Vessel Code Section XI, 2001 Edition, "Rules for In-service Inspection of Nuclear Power Plant Components."
- 7-3 Bamford, W. H., "Fatigue Crack Growth of Stainless Steel Reactor Coolant Piping in a Pressurized Water Reactor Environment," ASME Trans. Journal of Pressure Vessel Technology, February 1979.
- 7-4 James, L. A. and Jones, D. P., "Fatigue Crack Growth Correlations for Austenitic Stainless Steel in Air," in Predictive Capabilities in Environmentally Assisted Cracking, ASME publication PVP-99, December 1985.

Table 7-1 Surge Line Transients

Number	Transient Identification	Design Cycles
1	Pressurizer Heatup	200
2	Pressurizer Cooldown	200
3	Reactor Trip, Loss of Flow, Loss of Load	480
4	Plant Trips, Loading, and Unloading Down	30500
5	Plant Trips, Loading, and Unloading Up	30500
6	Plant Unloading, 10% Step Down	25000
7	Plant Unloading, 10% Step Up	25000
8	Hydrostatic Test, 3125 psia*	10
9	Leak Test, 2250 psi, Up	200
10	Leak Test, 2250 psi, Down	200
11	Insurge/Outsurge 1, DT = 50°F	120
12	Insurge/Outsurge 2, DT = 100°F	200
13	Insurge/Outsurge 3, DT = 150°F	480
14	Insurge/Outsurge 8, DT = 50°F	40
15	Insurge/Outsurge 9, DT = 100°F	160
16	Insurge/Outsurge 10, DT = 150°F	120
17	Insurge/Outsurge 11, DT = 200°F	120
18	Insurge/Outsurge 12, DT = 250°F	480
19	Insurge/Outsurge 13, DT = 300°F	360
20	Insurge/Outsurge 14, DT = 350°F	200
21	OBE	400
22	Thermal Stratification HU, $\Delta T = 320^\circ\text{F}$, LP	75
23	Thermal Stratification HU, $\Delta T = 320^\circ\text{F}$, HP	75
24	Thermal Stratification HU, $\Delta T = 250^\circ\text{F}$, LP	375
25	Thermal Stratification HU, $\Delta T = 250^\circ\text{F}$, HP	375
26	Thermal Stratification HU, $\Delta T = 200^\circ\text{F}$, LP	400
27	Thermal Stratification HU, $\Delta T = 200^\circ\text{F}$, HP	400

28	Thermal Stratification HU, $\Delta T = 150^\circ\text{F}$, LP	500
29	Thermal Stratification HU, $\Delta T = 150^\circ\text{F}$, HP	500
30	Thermal Stratification HU, $\Delta T = 90^\circ\text{F}$, Hot Standby	87,710
31	Thermal Stratification CD, $\Delta T = 320^\circ\text{F}$, LP	75
32	Thermal Stratification CD, $\Delta T = 320^\circ\text{F}$, HP	75
33	Thermal Stratification CD, $\Delta T = 250^\circ\text{F}$, LP	375
34	Thermal Stratification CD, $\Delta T = 250^\circ\text{F}$, HP	375
35	Thermal Stratification CD, $\Delta T = 200^\circ\text{F}$, LP	400
36	Thermal Stratification CD, $\Delta T = 200^\circ\text{F}$, HP	400
37	Thermal Stratification CD, $\Delta T = 150^\circ\text{F}$, LP	500
38	Thermal Stratification CD, $\Delta T = 150^\circ\text{F}$, HP	500
39	Thermal Stratification CD, $\Delta T = 90^\circ\text{F}$, Hot Standby	87,710

*Hydrostatic Test is considered as a pressure transient.

HU = Heatup

CD = Cooldown

HP = High Pressure

LP = Low Pressure

DT = Delta temperature (Temperature difference between the Pressurizer temperature and the Hot Leg temperature).

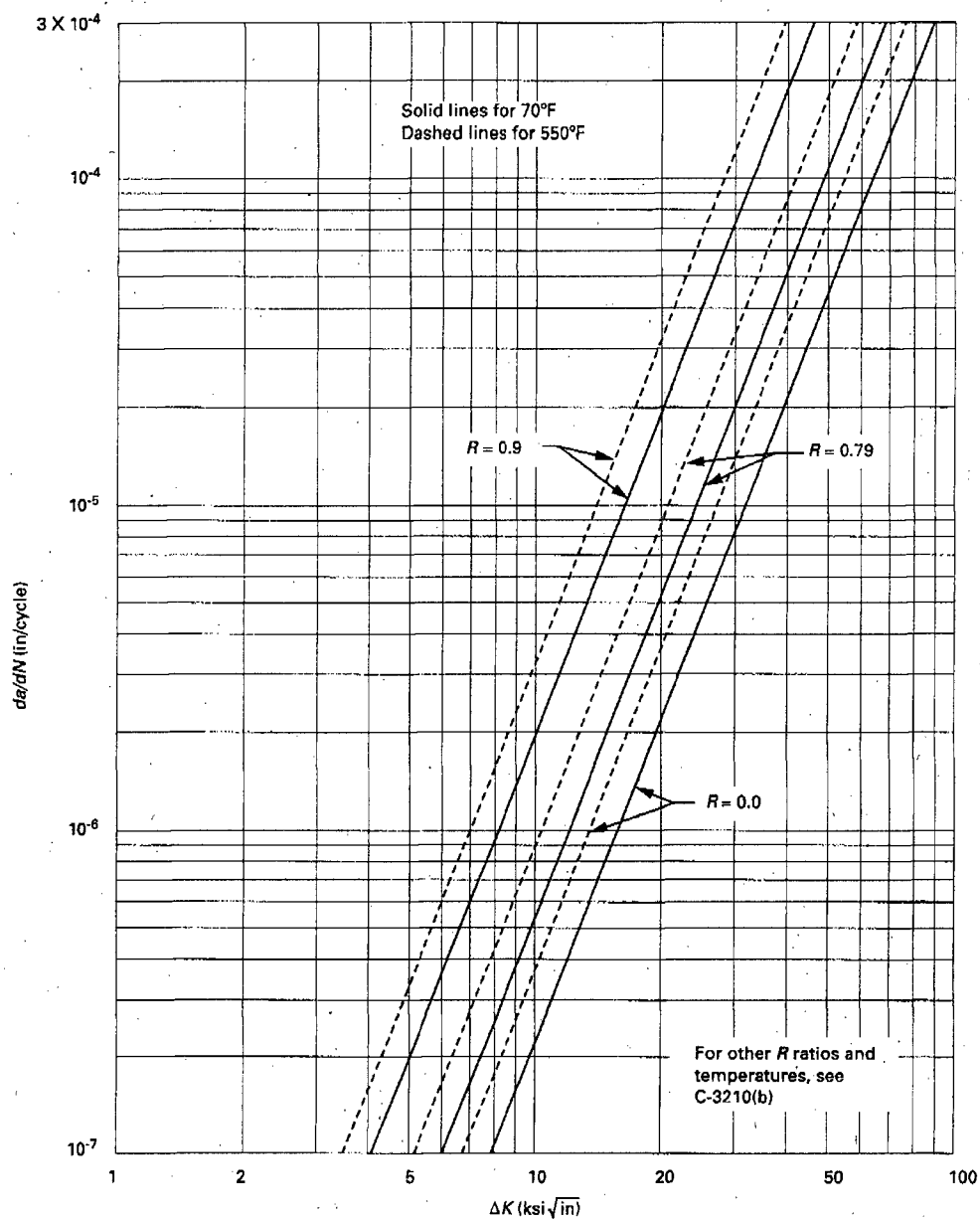
OBE = Operational Basis Earthquake

Table 7-2 FCG Results for Pressurizer Surge Line Nozzle Weld Overlay Region	
Flaw	Time for an Initial Flaw 75% of Original Thickness to Reach the Weld Overlay
Circumferential (DMW)	> 60 years [15 years] ^{Note 1}
Circumferential (SSW)	54 years [34 years] ^{Note 1}

Table 7-3 FCG Results for Hot Leg Surge Line Nozzle Weld Overlay Region	
Flaw	Time for an Initial Flaw 75% of Original Thickness to Reach the Weld Overlay
Circumferential (DMW)	28 years [> 60 years] ^{Note 1}
Circumferential (SSW)	16 years [19 years] ^{Note 1}

Note 1 – The unbracketed FCG results provided are taken from Reference 1. A subsequent FCG reanalysis was performed for Entergy by the weld overlay vendor. These results are provided in brackets.

Table 7-4 FCG Results for Intermediate Surge Line Location (Node 70)		
Flaw	Initial Flaw Size (% of wall thickness)	Final Flaw Size (% of wall thickness)
Circumferential	10%	38%



Note: A Factor of 2.0 is applied to the Air Environment Curve to Represent crack growth rate in PWR Environment

Figure 7-1 Reference Fatigue Crack Growth Curves for Stainless Steel

8.0 ASSESSMENT OF MARGINS

In the preceding sections, the leak rate calculations, fracture mechanics analysis and fatigue crack growth analyses were performed. In Section 6.3 using the SRP 3.6.3 approach (i.e., "Z" factor approach), the "critical" flaw sizes at the governing locations are calculated. Elastic-Plastic J-integral stability analyses are also performed in Section 6.3. In Section 5.4 the crack lengths yielding a leak rate of 2.5 gpm (10 times the leak detection capability of 0.25 gpm) for the governing locations are calculated. Margins at these locations are summarized below:

- Margin on Leak Rate:

A margin of 10 exists between the calculated leak rate from the leakage flaw and the leak detection capability of 0.25 gpm.

- Margin on Flaw Size:

Using faulted loads obtained by the absolute sum method, a margin of 2 or more exists between the critical flaw and the flaw having a leak rate of 2.5 gpm (the leakage flaw). The margins for analysis combination governing loading well exceed the factor of 2.

- Margin On loads:

The faulted loads are combined by absolute summation method and therefore the recommended margin on loads of 1.0 is satisfied as per SRP 3.6.3.

The leakage flaw sizes, the critical flaw sizes, and the margins are given in Tables 8-1, 8-2, and 8-3 for the critical surge line piping locations and governing Alloy 82/182 and Alloy 52M location. The margins are the ratio of critical flaw size to leakage flaw size. The J-integral stability margins based on the fracture toughness of the surge line pipe are provided in Table 8-3. Based on the results from these tables, it is concluded that all the LBB recommended margins are satisfied.

Node Location	Critical Flaw (in)	Leakage Flaw (in.)	Margin
70	10.5	3.18	3.3 ^a
	10.4	3.24	3.2 ^b
75	11.2	3.14	3.6 ^a
	11.1	3.2	3.5 ^b
20	12.6	3.1	4.1 ^a
	12.8	3.16	4.1 ^b

^a Based on base metal tensile properties.

^b Based on weld metal tensile properties.

Location	Critical Flaw Size (in)	Leakage Flaw Size (in)	Margin

a, c, e

Table 8-3 Stability Margins for Waterford 3 Pressurizer Surge Line Piping Based on Elastic-Plastic J-integral Evaluations			
Node	Flaw Size* (in.)	Leakage Flaw Size (in.)	Margin

a,c,e

9.0 CONCLUSIONS

This report justifies the elimination of Pressurizer surge line pipe breaks from the structural design basis for the Waterford 3 as follows:

- a. Stress corrosion cracking is precluded by use of fracture resistant materials in the surge line piping system and controls on reactor coolant chemistry, temperature, pressure, and flow during normal operation. A structural weld overlay was applied to mitigate PWSCC concern at the Alloy 82/182 weld location Waterford 3 Surge line to hot leg nozzle and the Pressurizer surge nozzle.
- b. Water hammer should not occur in the RCS piping (primary loop and the attached Class 1 auxiliary line) because of system design, testing, and operational considerations.
- c. The effects of low and high cycle fatigue on the integrity of the surge line were evaluated and shown to be acceptable. The effects of thermal stratification were evaluated and shown to be acceptable.
- d. Ample margin exists between the leak rate of small stable flaws and the capability of the Waterford 3 reactor coolant system pressure boundary leakage detection system (margin on leak rate of 10 was satisfied, see Tables 5-1 and 5-2).
- e. Ample margin exists between the small stable leakage flow sizes of item (d) and the critical flow sizes (see Tables 8-1 to 8-3 for a summary of margin).
- f. Fatigue crack growth analysis demonstrated that a through-wall crack will not result for the life of the plant at the highest stressed location.

The postulated reference flaw will be stable because of the ample margins in items (d) and (e), and will leak at a detectable rate which will allow a safe plant shutdown.

Based on the above discussion, it is concluded that the pressurizer surge line breaks should not be considered in the structural design basis for the Waterford 3.

APPENDIX A – LIMIT MOMENT

[

] a,c,e



Figure A-1 Pipe with a Through-Wall Crack In Bending